International Journal of Heat and Mass Transfer 164 (2021) 120566

Contents lists available at ScienceDirect

International Journal of Heat and Mass Transfer

journal homepage: www.elsevier.com/locate/hmt

Flow-solidification interaction: A numerical study on solidification of NH_4Cl – 70 wt.%H_2O solution in a water-cooled mould with a large sample thickness

Menghuai Wu*, Mihaela Stefan-Kharicha, Abdellah Kharicha, Andreas Ludwig

Chair for Modeling and Simulation of Metallurgical Processes, University of Leoben, Austria

ARTICLE INFO

Article history:
Received 23 April 2020
Revised 3 September 2020
Accepted 3 October 2020

Keywords:
Flow-solidification interaction
Mushy zone
Freckle
Macrosegregation
Volume average

ABSTRACT

This study focuses on the flow-solidification interaction during the solidification of NH_4Cl – 70.43 wt.%H_2O solution in a water-cooled mould with a large sample thickness (100 × 80 × 10 mm^3). First part of the paper is to use a volume-average-based dendritic solidification model to reproduce an experiment in which transient flow is monitored in-situ using particle image velocimetry, and the solidification sequence is recorded with a light camera. The striking features of the solidification experiment are that the crystal morphology is dominant in a columnar structure, and four typical flow regimes appear in the bulk solution during cooling/solidification, namely pure thermal convection, unstable turbulent flow caused by double diffusive convection, turbulent-stratified flow, and meandering flow. The results show that there is quantitative agreement between the simulation and experiment results. The focus of this paper (second part) is to study the flow-solidification interaction by correlating the above flow regimes with the solidification quantities in the mushy zone. Owing to the enhanced mass (solute) and energy transport by advection, flow suppresses the growth of the mushy zone, while speeding up the solidification inside the mushy zone, leading to the formation of dense mush and massive columnar dendrite trunks. The crystalline morphology of NH_4Cl, as presented by a dendritic envelope and described by morphological parameters, is an important factor that influences the flow; as a feedback, the flow further influences the solidification inside the mushy zone. The numerical model also provides valuable information about the formation of freckle trails.

1. Introduction

Although the art of making casting is several thousand years old, the flow-solidification interaction in the advancing mushy zone and its impact on the casting quality, as characterized by the as-solidified microstructure and accompanying defects, remain relatively unknown. The flow may play a more important role than the thermal fields in the development of the mushy zone, induction of macrosegregation, and modification of the crystalline dendritic morphology through coarsening/ripening; in turn, the advancing mushy zone can dampen the flow or modify the flow pattern.

Based on the transparent analogues (e.g., aqueous solution of ammonium chloride, NH_4Cl – H_2O), the method of in-situ observation of the flow during solidification was first introduced in the 1970s to investigate the formation of channel segregates/freckles [1–3]. Channel segregates/freckles are a typical casting defect, as found in many engineering castings, and they were believed to have been the direct result of the flow-solidification interaction in/near the mushy zone; this was subsequently verified by many follow-up studies [4–6]. Nowadays, the in-situ observation of the solidification of the metal alloys using X-ray radioscopy or synchrotron X-ray radiography has been made possible, and it was applied to study the formation of plumes/chimneys, i.e., the onset of freckles or channel segregates [7–9]. One drawback of the X-ray techniques is that the solidification sample has to be limited to a thickness of 100 ~ 150 μm (Hele-Shaw cell). With this limitation, the three-dimensional (3D) nature of the flow dynamics, which plays a crucial role in some engineering castings, cannot be properly investigated. Therefore, NH_4Cl – H_2O solutions are still used to study the formation mechanism of freckles in 3D samples, e.g., under the modified flow condition [10] and under the static

* Corresponding author.
E-mail address: menghuai.wu@unileoben.ac.at (M. Wu).

https://doi.org/10.1016/j.ijheatmasstransfer.2020.120566

magnetic field [11]. The NH_4Cl – H_2O solution was also used to study the equiaxed solidification, where the motion of crystals is of primary interest [12–14]. The significant advantages of the experiments with NH_4Cl – H_2O solution are that (1) the solidification sample can be designed in a dimension relevant to engineering castings, and (2) the recently developed particle image velocimetry (PIV) technique allows the transient flow field to be monitored with good quantitative accuracy.

A recent experiment has monitored the flow dynamics using the PIV technique during solidification of the NH_4Cl – H_2O solution in a water-cooled mould with a large sample thickness (10 mm) [15]. Interestingly, four flow regimes were observed in the bulk solution during cooling/solidification, namely pure thermal convection (TH), unstable/turbulent flow (TU), turbulent-stratified flow (TU-ST), and meandering flow (MF). The thermal and solutal Rayleigh number (R_a) in different flow regimes were analysed [13,15]. For a vertical wall, the critical R_a for the occurrence of turbulence is 10^9. In the TH stage the R_a is too small (~10^8) to induce a transition from laminar to turbulence. As soon as solidification starts (stages TU and TU-ST), the solutal buoyancy becomes dominant, and the R_a reaches 1.32×10^{10}. The flow is highly instable and turbulent. The aforementioned four flow regimes in this experiment correspond to different cooling/solidification stages and were assumed to reflect their interactions with the developing mushy zone. In order to explain above flow regimes corresponding to the evolution of the solidifying mushy zone, a numerical modelling study is needed. The in-situ observed experimental information is not sufficient for that purpose.

The volume-average-based multiphase approach, which was first introduced by Beckermann et al., was successfully used to model the solidification problem by bridging the transport phenomena at different length scales [16–17]. The concept of a 'dendrite envelope', as proposed by Rappaz et al. [18-19], was incorporated into the volume-averaged approach by Wang and Beckermann to consider the dendritic crystal morphology [20]. Recently, this work was extended by Wu and Ludwig to consider the mixed columnar-equiaxed solidification in a five-phase solidification model [21–22]. This model was also partially evaluated against the in-situ solidification experiments on organic materials [23] and against metal castings [24–25]. It is worth mentioning that large numbers of pioneering works have be devoted to the flow-solidification interaction issue, using volume-average-based or similar approaches, with most emphasis on the freckle formation in the mush zone [26-29]. The freckle is a typical phenomenon of many engineering castings and it is the outcome of the flow-solidification interaction in/near the mushy zone. The interested readers are referred to some previous and recent reviews of this topic [4, 16-17, 30].

The objective of the current work is to simulate the in-situ solidification experiment using an NH_4Cl – H_2O solution with the five-phase volume-average-based dendritic solidification model [15]. A part of the study on the simulation-experiment comparison is to be presented at a conference [31]. This paper focuses on the analysis of the flow-solidification interaction, and hence aims to improve the understanding of the embedded mechanisms related to the formation of the as-solidified structure and freckle trails.

2. Experimental setup

The solidification experiment with the NH_4Cl – 70.43 wt.%H_2O solution was published previously [15]. As shown in Fig. 1(a), the dimension of the mould cavity is $100 \times 80 \times 10$ mm^3. The side/bottom walls (copper) of the mould were water-cooled; the front/back walls (glass plates) were isolated; the top surface was open to the air. The NH_4Cl – H_2O solution was poured in the mould and heated initially, after which it was maintained at a constant temperature T_0 (314.15 K) until the solution became quiescent. Cooling started by circulating the cooling water in the copper mould and the cooling history of the side/bottom walls was monitored with instrumented thermal couples (C1 – C3), as shown in Fig. 1(b). Thermocouples, as marked in Fig. 1(a), are instrumented inside the mould and 5 mm from the mould/cell interface. The particle image velocimetry (PIV) technique was used to record the flow dynamics on the large symmetry plane of the cell. A solidification front of the mushy zone was recorded by a light camera. The image from the light camera could also give some indication about the solid phase distribution in the mushy zone through its brightness, i.e. the brighter region corresponds to the location where the solid phase is less densely distributed.

3. Numerical model and simulation settings

The mixed columnar-equiaxed solidification model developed by the current author considers five phases [21–22, 30]. As a dominant columnar dendrite structure of NH_4Cl is observed in this experiment, a simplified version with columnar (dendritic) growth is applied. Two hydrodynamic phases are considered: the primary melt (ℓ) and columnar phase (c), and their volume fractions sum up to a unit ($f_\ell + f_c = 1.0$). The columnar phase includes the solid dendrites and enclosed interdendritic melt. As shown in Fig. 2, a hypothetical contour connecting primary (or secondary and tertiary) dendrite tips, which is called a dendrite envelope, is constructed to separate the inter-dendritic melt from the primary or extra-dendritic melt. Following this concept, the system includes three model phases: the solid dendrites (f_s^c), the inter-dendritic melt inside the envelope (f_d^c), and the extra-dendritic melt (identical to the primary melt f_ℓ), where $f_s^c + f_d^c = f_c$. The volume fraction of the solid (or interdendritic melt) inside the envelope is $\alpha_s^c = f_s^c/f_c$ (or $\alpha_d^c = f_d^c/f_c$). The shape of the columnar dendrite envelope is further simplified as a volume-equivalent cylinder; the contour of the dendrite envelope near the primary dendrite tip is simplified as a paraboloid. Assuming that the growth kinetics of the dendrite tips follows the Lipton-Glicksman-Kurz model [32],

$$v_{tip}^c = \frac{4.0 \cdot \sigma^* \cdot D_\ell \cdot m_\ell \cdot c_\ell^* \cdot (k-1)}{\Gamma} \left(Iv^{-1}(\Omega)\right)^2 \quad (1)$$

where the stability constant (also called as selection constant) is $\sigma^* = 1/(4\pi^2)$ and Ω is the compositional undercooling $(c_\ell^* - c_\ell)/(c_\ell^* - c_s^*)$. We assume that v_{tip}^c above applies for both $v_{tip'}^c$ and $v_{tip''}^c$. From the growth velocity of the primary dendrite tip ($v_{tip'}^c$), one can track the columnar primary dendrite tip front explicitly [30]. Two morphological parameters are necessarily defined to describe the geometry of the dendrite envelope: the shape factor $\Phi_{env}^c$and circularity factorΦ_{circ}^c. From the tip growth velocity of the secondary dendrite tips ($v_{tip''}^c$), one can calculate the lateral growth velocity of the volume-equivalent cylinder:

$$v_{env}^c = \Phi_{env}^c \cdot v_{tip''}^c. \quad (2)$$

The diffusion area of the columnar envelope ($S_{env,D}^c$) is estimated according to the surface area of the volume-equivalent cylinder ($S_{env,M}^c$) by considering a circularity factor Φ_{circ}^c, where

$$S_{env,D}^c = S_{env,M}^c / \Phi_{circ}^c. \quad (3)$$

Here, the shape factor and the circulatory factor are assumed, and they are further verified for this experiment for each numerical parameter study: Φ_{env}^c= 0.7979, Φ_{circ}^c= 0.33. From v_{env}^c and $S_{env,M}^c$, one can calculate the growth rate of the columnar dendrite envelope, i.e., the mass transfer rate from extra-dendritic melt into inter-dendritic melt$M_{\ell c}$.

The solidification rate of the interdendritic melt (M_{ds}^c) is determined by the growth velocity of the interface between the solid

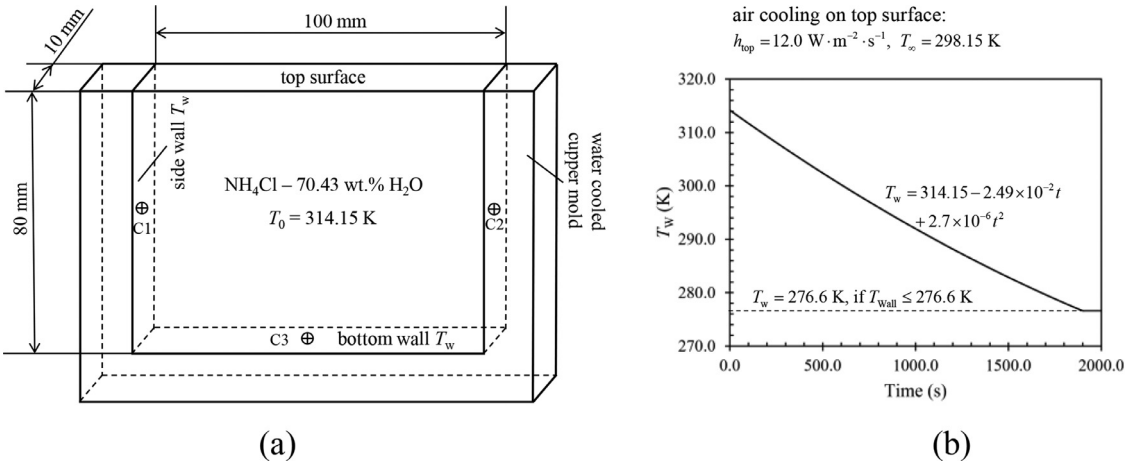

Fig. 1. Sketch of the experimental setup (a) and cooling conditions on mould walls (b). The front/back glass walls (plates) can be treated as adiabatic.

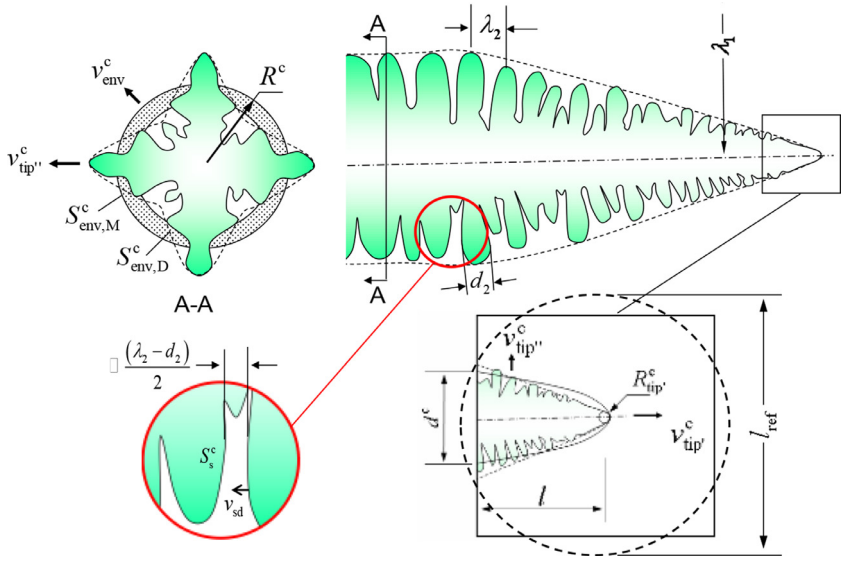

Fig. 2. The columnar dendrite envelope (dashed line), which connects the secondary and tertiary dendrite tips, is simplified as a volume-equivalent cylinder (solid line, A-A). The contour of the columnar envelope near the primary dendrite tip (dashed line connecting the primary and secondary dendrite tips) is simplified as a paraboloid (solid line).

dendrite and the interdendritic melt v_{sd} and its interface area concentration S_s^d. Solidification of the interdendritic melt is driven by supersaturation, $(c_\ell^* - c_d^c)/(c_\ell^* - c_s^*)$, and it is governed by solute diffusion in the interdendritic melt region. The diffusion length in the interdendritic melt $l_d$is related to the secondary dendrite arm spacing λ_2 by $l_d = \beta_2 \cdot (\lambda_2 - d_2)/2$, where β_2 is a constant of the order of unity, and d_2 is the diameter of the secondary dendrite arms. It is assumed that d_2 is correlated to λ_2 by $\lambda_2 - d_2 = \lambda_2 \cdot \alpha_d^c$. Thus,

$$v_{sd} = \frac{2 \cdot D_\ell}{\beta_2 \cdot \lambda_2 \cdot \alpha_d^c} \cdot \frac{c_\ell^* - c_d^c}{c_\ell^* - c_s^*} \tag{4}$$

The interface area in an enclosed dendrite envelope is also related to the secondary dendrite arm spacing ($\propto 2/\lambda_2$). Considering an impingement factor Φ_{Imp}^s ($=\alpha_d^c$), the interface area concentration, with reference to the total volume, can be calculated as

$$S_s^d = \frac{2 \cdot \Phi_{Imp}^s}{\lambda_2} \cdot f_c. \tag{5}$$

Only one set of Navier-Stokes equations are solved to determine the velocity of the primary or extra-dendritic melt ($\vec{u}_\ell$); the columnar phase is stationary ($\vec{u}_c$= 0.0). The mushy zone is treated as a permeable porous medium which is constructed with dendrite network filled with liquid channels. The flow permeability (K) of the mushy zone depends on both liquid volume fraction and the character length of the dendritic structure. When considered isotropic, referring to Ramirez et al. [33], the permeability tensor reduces to a scalar value:

$$K = \frac{\lambda_1^2 f_\ell^3}{1667(1 - f_\ell)^2} \tag{6}$$

where λ_1 is the primary dendrite arm spacing. To study its influence on the flow, an alternative permeability formulation [34] is used for the numerical parameter study:

$$K = \frac{\lambda_2^2 f_\ell^3}{20\pi^2(1 - f_\ell)^2} \tag{7}$$

where λ_2 is the secondary dendrite arm spacing. As both λ_1 and λ_2 are assumed constant during solidification, the permeability calculated by Eq. (7) is ca. 1/4 of the one by Eq. (6). Further discussion on the permeability is made in the discussion section (§.6).

For further modelling details, global transport equations, and solution strategy, refer to [21–22, 30]. The calculation domain, which is 100 × 80 × 10 mm^3, is shown in Fig. 1(a). The thermal

Table 1
Material properties and other parameters.

	Symbol	Units	Value	Sources
Thermodynamic parameter (local linearized phase diagram)				
Nominal concentration	c_0	wt.% H_2O	70.43	[35]
Liquidus temperature	T_{liq}	K	304.15	[35]
Melting point of solvent	T_f	K	638.7	extrapolation
Eutectic composition	c_{eu}	wt.%	80.3	[35]
Eutectic temperature	T_{eu}	K	257.267	[35]
Liquidus slope	m	K (wt.%)$^{-1}$	−4.75	[35]
Equilibrium partition coefficient	k	–	0.0	[35]
Gibbs Thomson coefficient	Γ	K.m	4.0×10^{-8}	[36]
Thermo-physical properties				
Reference density	ρ_ℓ, ρ_s	kg $\cdot$ m^{-3}	1073	[37]
Specific heat	c_p^ℓ,c_p^s	J kg^{-1} K^{-1}	3249	[12]
Thermal conductivity of liquid	k_ℓ	W m^{-1} K^{-1}	0.468	[12]
Thermal conductivity of solid	k_s	W m^{-1} K^{-1}	2.7	[12]
Latent heat	Δh_f	J kg^{-1}	3.18×10^5	[12]
Viscosity	μ_ℓ	Kg m^{-1} s^{-1}	1.3×10^{-3}	[12]
Diffusion coefficient (liquid)	D_ℓ	m^2 s^{-1}	4.8×10^{-9}	[12]
Boussinesq parameters				
Liquid thermal expansion coefficient	β_T	K^{-1}	3.9×10^{-4}	[37]
Liquid solutal expansion coefficient	β_C	wt.%$^{-1}$	2.87×10^{-3}	[37]
Dendrite morphology				
Primary dendritic arm spacing	λ_1	m	6.0×10^{-4}	[15]
Secondary dendritic arm spacing	λ_2	m	1.0×10^{-4}	[15]

Table 2
Numerical parameter study.

Simulation cases		Description
Ia	with flow	This is a reference case; all simulation settings are described in §2–3.
Ib	without flow	
IIa	with flow	Identical to Case I, but the shape factor of the columnar dendrite envelope Φ^c_{env} is changed to 0.399 (0.7979 for Case I).
IIb	without flow	
IIIa	with flow	Identical to Case I, but the circularity factor of the columnar dendrite envelope Φ^c_{circ} is changed to 0.67 (0.33 for Case I).
IIIb	without flow	
IVa	with flow	Identical to Case I, but the permeability of the mushy zone is modified according to Ref. [34] using Eq. (7). Eq. (6) was used for Case I.

boundary condition is shown in Fig. 1(b). For the flow, non-slip boundary conditions were applied for all walls except for the top surface (free-slip). In addition, solidification shrinkage is ignored, and the Boussinesq approximation is made for the thermo-solutal buoyancy flow. Material properties are listed in Table 1. The primary and secondary dendrite arm spacings ($\lambda_1$andλ_2) were determined experimentally. Seven simulation cases were defined in Table 2. All simulations were made in full 3D with a mesh size of 0.7 mm. Following Felicelli et al. [26-27], some flow-interaction phenomena such as the formation of channel/freckle are typical three directional, and they can only be well resolved in 3D simulation.

4. Solidification sequence: simulation vs. experiment

Results of a section of the simulation-experiment comparison study have been presented at a conference [31]. This paper focuses on the theoretical analysis of flow-solidification interaction. A comparison of experimental results with the calculated solidification sequence and flow patterns for the reference Case Ia is shown in Fig. 3. Fig. 4 shows the following solidification quantities: temperature (T_ℓ), solute (H_2O) concentration in the melt (c_ℓ in mass fraction), density of the melt (ρ_ℓ), and volume fraction of the solid dendrite (f_s^c). As measured in the experiment [15], four typical bulk flow regimes were successfully reproduced by the numerical model. The time of the starting point for each flow regime was predicted to be slightly different from that of the experiment because the thermal boundary conditions as applied for the simulation were not perfectly in agreement with the real condition. It was assumed that the temperatures on cell-mould interfaces (side and bottom) are uniform, and they are determined by thermocouples (C1 – C3), as shown in Fig. 1(a). The temperature at the corner may be different from that on the middle cell-mould interface. Another assumption, i.e. adiabatic for the front and back (glass) walls, may also cause error.

As shown in Fig. 3(a), the thermal convection regime corresponds to the early cooling stage before solidification. The flow is laminar and symmetrical. Note that the PIV technique is not able to detect the velocity near the side wall; hence, the largest velocity along the side walls, as calculated by the simulation, cannot be detected experimentally.

The turbulent regime (TU) corresponds to the start of solidification. As shown in Fig. 3(b), NH_4Cl crystals grow from the side/bottom walls. The mushy zone is very porous; the maximum f_s^c is about 0.12. The rejection of solute (H_2O) in the mushy region leads to the 'density reversion' [2], i.e., the melt density along the side wall becomes lighter than that in the bulk region. Then, at 900 s, the flow direction along the side wall reverses. The temperature along the side wall is lower, while the solute concentration (H_2O) is higher, Fig. 4(a1)-(a4). The solute rejection from the mushy zone along the bottom wall leads to rising plumes, i.e., the onset of freckle trails. A typical double-diffusive convection pattern occurs. At this moment, the flow pattern becomes chaotic.

As the solidification proceeds to ca. 1380s, as shown in Fig. 3(c), a turbulent – stratified flow (TU-ST) forms. The bulk flow is divided into two parts: the lower part is similar to the previous TU region, i.e., chaotic with coherent structures, while the upper part starts a stratification with two circulation loops. The upward melt flow in the mushy zone along the side wall continuously brings the lighter melt (segregated with H_2O) from the lower to the upper parts, leading to a separation of the bulk melt into two parts,

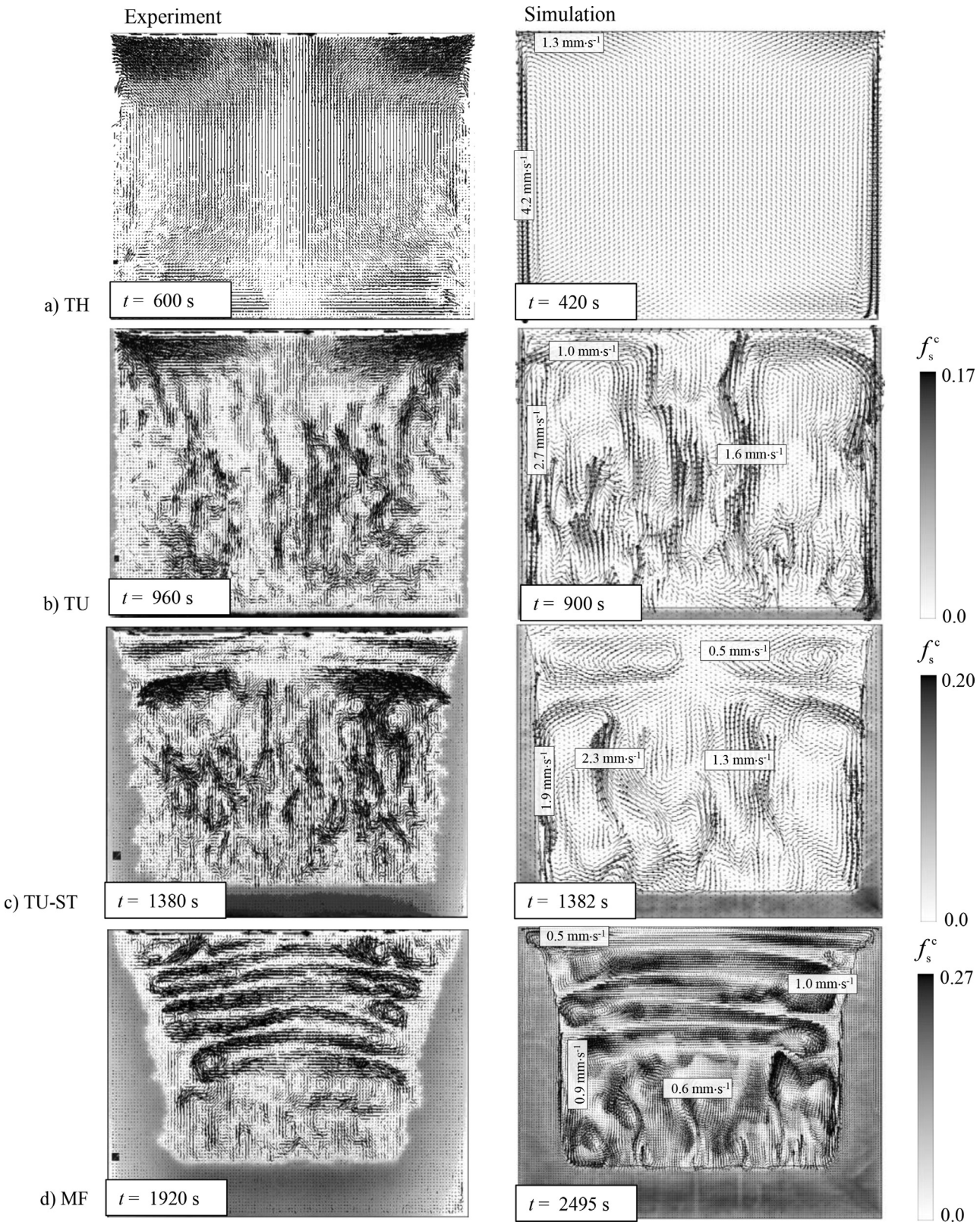

Fig. 3. Solidification sequence and flow patterns (Case Ia): simulation-experiment comparison. Experiment (left): the grey area represents the mushy zone and vectors for the measured velocity field using the PIV technique. Simulation (right): grey scale represents f_s^c (volume fraction of solid dendrites) and vectors for the liquid velocity $\vec{u}_\ell$. Four different flow patterns, which correspond to four different cooling/solidification stages, are: a) TH (thermal convection), b) TU (turbulence), c) TU-ST (turbulence–stratified flow), and d) MF (meandering flow). All of the simulation results and the flow measurement (flow) were obtained from the large symmetry section.

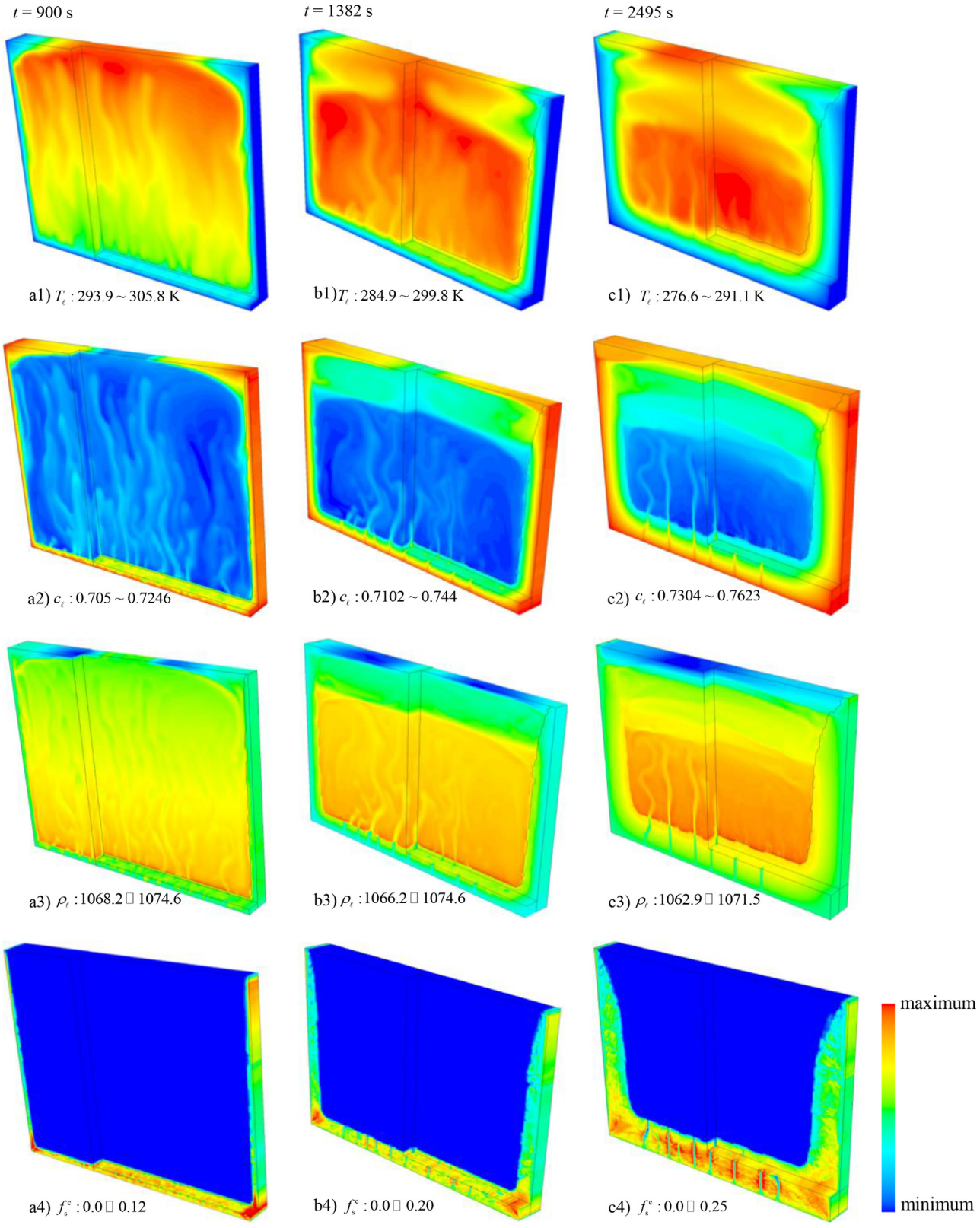

Fig. 4. Some key solidification quantities (T_ℓ,c_ℓ,ρ_ℓ,f_s^c) for Case Ia are shown in a sequence at 900, 1382, and 2495s. The results are shown in 3D; therefore, one can only see the distribution of each quantity in selected sections. All quantities are shown in the colour scale with blue and red for the minimum and maximum values, which are given below each figure. (For interpretation of the references to colour in this figure legend, the reader is referred to the web version of this article.)

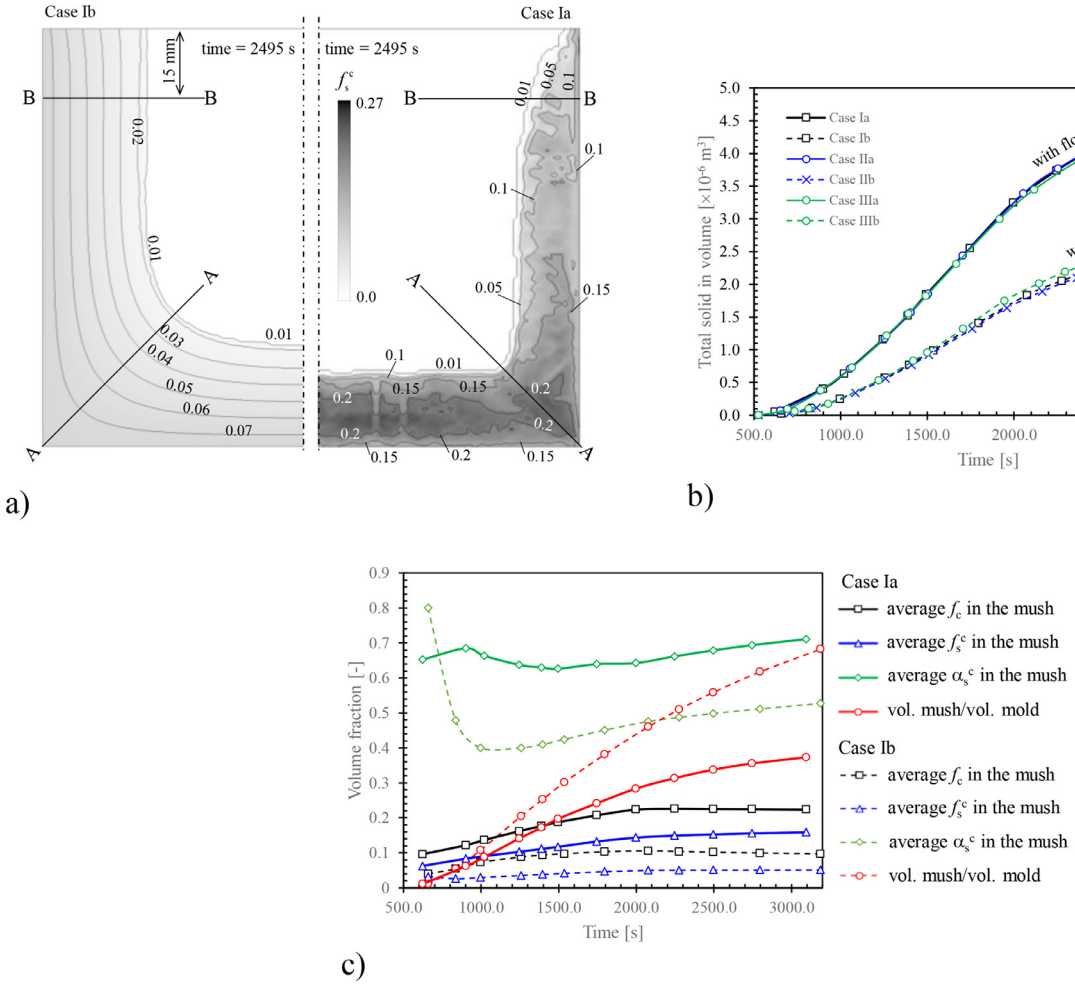

Fig. 5. Effect of the flow on the mushy zone: Case Ia (right half, with flow) vs. Case Ib (left half, without flow). (a) f_s^c contours on the symmetry plane in grey scale and isolines (t = 2495s); (b) evolution of total solid in the entire mould volume ($\iiint f_s^c dV$); (c) evolution of average f_c, f_s^c, and α_s^c in the mush and the volume ratio of the mush over the entire mould. As a comparison, other simulation cases are also shown in Fig. 5(b).

Fig. 4(b1)-(b4). The upper part is lighter and the lower part is denser. Along the bottom wall, plumes continue to develop. The non-uniform distribution of f_s^c in the simulation result shows the freckle trails [2]. The plumes in the experimental result appear to indicate the freckle trails, but no clear freckle trail is seen in the mush. The small difference in f_s^c in and surround freckle trails may not be detected by the light camera.

A meandering flow (MF) develops during the late stage of solidification, as shown in Figs. 3(d) and 4(c1)-(c4). The stratification flow in the upper part is gradually organized horizontally in several layers. The upper region of the lighter melt becomes broader; several circulation loops appear from two sides of the mould. The circulation loops from two sides are gradually merged, and the flow pattern is rearranged to form the MF. The experiment appears to show more flow layers than those of the simulation, which may be because the numerical grid resolution is not sufficiently high.

5. Flow-solidification interactions

5.1. Effect of the flow on the mushy zone

In order to understand the flow effect on the mushy zone evolution, two simulations are made: Case Ia considering the thermo-solutal convection, and Case Ib considering a pure diffusive case without any flow. Fig. 5(a) shows the solidification profile (f_s^c distribution) on the symmetry plane at 2495s. The mushy zone of Case Ia is significantly smaller than that of Case Ib. The mushy zone thickness (depth) is reduced by the flow, i.e., the flow hinders the growth of columnar primary dendrite tips. However, the mushy zone of Case Ia is denser than Case Ib, i.e., f_s^c in Case Ia is higher than that of Case Ib. In Case Ib, f_s^c contours are more uniformly distributed, while in Case Ia, f_s^c contours are irregular. By summing up all solid phases (f_s^c) over the entire mould volume, i.e., performing $\iiint f_s^c dV$, one obtains the time evolution of the total solid (Fig. 5(b)): Case Ia solidifies much faster than Case Ib. Some volume-averaged quantities as a function of time are shown in Fig. 5(c). The total volume of the experiment cell is V; the volume of the mush zone region is V_{mush}. The volume fraction of the columnar dendrite envelope f_c averaged in the mush region (black curves) is calculated as $\iiint f_c dV/V_{mush}$; The volume fraction of solid f_s^c averaged in the mush region (blue curves) is calculated as $\iiint f_s^c dV/V_{mush}$; The solid fraction inside the envelope α_s^c averaged in the mush region (green curves) is calculated as $\iiint \alpha_s^c dV/V_{mush}$. The volume ratio of the mush zone region over the entire mould is calculated as V_{mush}/V. The growth of the columnar dendrite envelope (f_c black lines) and the solidification of NH_4Cl crystals (f_s^c blue lines) averaged in the much zone region are much faster in Case Ia than those in Case Ib. In addition, the solid fraction inside the dendrite envelope (α_s^c green lines) averaged in the mush zone region in Case Ia is also larger (the columnar trunk is more massive) than that in Case Ib. The red lines in Fig. 5(c) show the ratio of the total volume of the mushy zone to the entire mould vol-

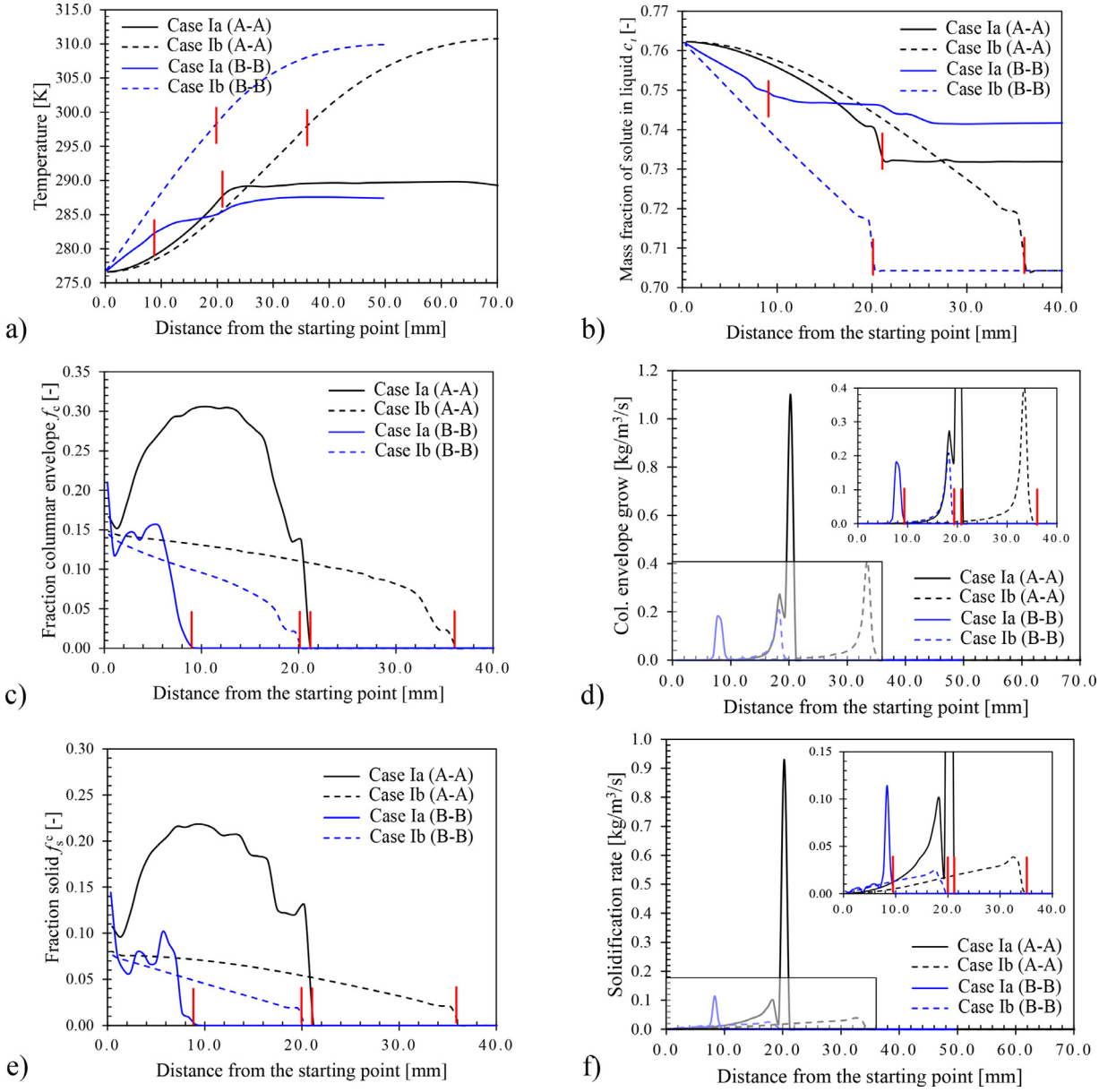

Fig. 6. Effect of flow on the solidification parameters along two lines, A-A and B-B (made on the symmetry plane) as marked in Fig. 5(a) - comparison between Case Ia (with flow) and Case Ib (without flow). (a) Temperature T, (b) mass fraction of solute (H_2O) in the melt c_ℓ, (c) volume fraction of columnar dendrite envelope f_c, (d) growth rate of the columnar dendrite envelope, or mass-transfer rate from extra-dendritic melt into inter-dendritic melt$M_{\ell c}$, (e) fraction solid f_s^c, (f) solidification rate of the interdendritic meltM_{ds}^c. Red bars as marked on different curves indicate the positions of the columnar dendrite tip front; t = 2495s.

ume. It expresses the same result of Fig. 5(a) in a different way, i.e., the flow reduces the mushy zone. The flow tends to hinder the growth of the columnar primary dendrite tips and reduce the mushy zone thickness, but the flow speeds up the solidification inside the mushy zone and leads to the formation of more massive columnar dendrite trunks.

Some solidification quantities along two lines, A-A and B-B as marked in Fig. 5(a), are presented in Fig. 6. These results, together with the solidification sequence of Fig. 4, further explain the effect of the aforementioned flow on the solidification. As shown in Figs. 6(a) and 4(c1), at 2495s, most superheat in the bulk melt is released through advection heat transfer (Case Ia), while a large amount of superheat remains in the bulk melt when no flow is present (Case Ib). The positions of the columnar primary dendrite tip front are marked with red lines (short red bars). The corresponding temperatures at the columnar tip positions are very different for the two cases, and they even vary with position when flow is present. The main reason is that the flow causes significant solute enrichment (c_ℓ) in the bulk melt, Figs. 6(b) and 4(c2), which reduces the local liquidus temperature. However, in the pure diffusive case (Case Ib), solute enrichment in the bulk is negligible and the columnar tip positions are located at a temperature of ca. 298.5 K, i.e., 5.65 K (undercooling) below the initial liquidus. The phase distributions, $f_c$in Fig. 6(c) and f_s^cin Fig. 6(e), are highly nonuniform for Case Ia: there are relatively low volume fractions near the casting surface/corner and relatively high volume fractions in the middle-distance regions between the solidification front and casting surface/corner. Without flow (Case Ib), both f_c and f_s^cincrease monotonically from the solidification front towards the surface/corner. The above phase distributions in the mushy zone can be explained by the growth rate of the columnar dendrite envelope$M_{\ell c}$ in Fig. 6(d) and the solidification rate

M^c_{ds} in Fig. 6(f). In principle, the largest $M_{\ell c}$ and M^c_{ds} occur near the columnar tip front for both cases. However, for Case Ia (flow), both$M_{\ell c}$and M^c_{ds} are accumulated near the columnar tip front (Case Ia), while for Case Ib, they reduce gradually from the columnar tip front towards the casting surface/corner. Further discussions are made in section §5.3.

As seen in Figs. 6(e) and 4(c4), an additional flow effect is the phase distribution (f^c_s) between lower (A-A) and upper (B-B) parts of the casting. A larger number of solid phase forms in the lower part compared with the upper part. The global flow pattern was described in the previous section (§4); the bulk melt enters the mush from the bottom/corner region, then rises along the side wall and returns to the upper part of the bulk region. The flow brings solute-enriched melt from the bottom mushy zone along the side wall to the upper part. This kind of flow modifies the melt concentration distribution (c_ℓ) (Fig. 4(c2), Fig. 6(b)). Compared with Case Ib, c_ℓ is significantly reduced along A-A (in the lower part) and it is enhanced along B-B (in the upper part) by the flow (Case Ia). $c_\ell$is a key parameter that influences the growth of the columnar dendrite envelope ($M_{\ell c}$) and solidification of the interdendritic melt (M^c_{ds}).

5.2. Effect of the mushy zone on the flow

The mushy zone is modelled as a solid-liquid mixture, where the solid phase is enclosed in an envelope whose shape is described by two model input parameters (Fig. 2): the shape factor Φ^c_{env} and circularity factorΦ^c_{circ}. Φ^c_{env} correlates the growth of the envelope with the dendrite tip growth kinetics [30], and hence impacts the calculation of f_c (orf_ℓ); Φ^c_{circ} aids in determining the surface area of the envelope, and hence impacts the calculation of the melt concentration (c_ℓ). In this sense, Φ^c_{env} and Φ^c_{circ}should influence the flow because the mush permeability (K) depends largely onf_ℓ, and the melt density ρ_ℓ (i.e., the buoyancy term) depends on c_ℓ. In Case I, Φ^c_{env}(= 0.7979) was taken from Ref. [21] by considering the cross section of the columnar dendrite envelop as a square rod; Φ^c_{circ}(= 0.33) was determined by performing a parametric study by fitting a numerically simulated solidification sequence and flow pattern with the experimental results (Fig. 3). In order to understand the impact of Φ^c_{env} and Φ^c_{circ} on the flow, two more simulation cases (Table 2) are defined as: (1) Case IIa by reducing $\Phi^c_{env}$from 0.7979 to 0.399, and (2) Case IIIa by increasing $\Phi^c_{circ}$from 0.33 to 0.67. Reducing Φ^c_{env} implies the slowing down of the envelope growth (Eq. (2) and Fig. 2); increasing Φ^c_{circ}means the reduction of the envelope diffusion area (Eq. (3) and Fig. 2).

Simulations for the pure diffusive cases are also performed: Case IIb and IIIb, which is compared with Case Ib. The influence of the morphological parameters on T, c_ℓ, and f^c_s appears to be very minor, but their influence on f_c is significant. Reducing Φ^c_{env} in Case IIb slows down the envelope growth, and hence there is a smaller f_c compared with that of Case Ib. Increasing Φ^c_{circ}in Case IIIb reduces the envelope diffusion area, and hence slows down the solute enrichment in the melt and in favour of the envelope growth. Fig. 5(b) shows the total as-solidified phase in the mould as a function of time, and all cases with and without flow are compared. With the exception of Case IIIb, all other cases are similar, implying that the total solidification rate in the system is mainly controlled by the cooling boundary condition, and it is independent of the above morphological parameters. By increasing Φ^c_{circ}, the total solid is slightly increased for the pure diffusive case (Case IIIb), while it is slightly decreased when the flow is activated (Case IIIa).

Modelling results on the flow and solidification sequence for the above cases are compared in Fig. 7. An additional case (Case IVa) is added here by considering an alternative permeability (K) law [34], i.e., Eq. (7). Given λ_2 (100 μm) in Table 1, the calculated permeability (Eq. (7)) is about 1/4 of that according to Eq. (6) in Case Ia. Fig. 7 shows only three late stages of solidification, corresponding to three late flow regimes (TU, TU-ST, and MF). The first flow regime (TH), which corresponds to the initial thermal convection before solidification, is not shown. At first glance, all cases show quite similar flow behaviors, and they can capture three typical flow regimes, as what were observed experimentally (Fig. 3). However, details about their behaviors are different. Actually, the MF (at 2495s) as observed in the experiment is best 'reproduced' by Case Ia. Case IIa shows some similarities of the MF, but its agreement with the experiment is not as good as Case Ia. This indicates that the flow is sensitive to the aforementioned morphological parameters and the mush permeability. The authors have actually performed more simulations by varying the above parameters compared with what is listed in Table 2. It is found that it is almost impossible for simulations with parameters that are different from the range of parameters given in Table 2 to reproduce the experimentally measured flow pattern in Fig. 3.

To get more insight into the formation of the MF, the temperature (T) and liquid concentration (c_ℓ) fields for the moment of 2495s are shown in Fig. 8, and a comparison between all cases (Case Ia - IVa) is made. Evolution of the T and $c_\ell$fields (only for Case Ia) can be found in Fig. 4. Both T and c_ℓ serve as the driving force (buoyancy) for the bulk flow. The solute-enriched melt (high c_ℓ), as emanated from the upper part of the mushy zone (side walls), tends to float on the top, building up the stratification. The melt with initially high temperature is 'pushed' downwards below the stratification. The role of $c_\ell$in the buoyancy force overwhelms that of T. As seen in Fig. 4, the stratification flow does not build up MF directly, but it firstly creates several circulation loops from two sides of the mould region. During the late stage of solidification, the circulation loops from both sides are merged/rearranged to form the MF. The stratification flow in the upper part is consistently interacting with, or disturbed by, the plumes coming from the bottom mushy zone. The plumes originate from the freckle trails of the bottom mushy zone (Section 5.3). The interaction between the stratification and the plumes explains the sensitivity of the MF formation to the morphological parameters (Φ^c_{env} and Φ^c_{circ}) and the mush permeability (K). The numbers and the flow intensity of the plumes depends on Φ^c_{env}, Φ^c_{circ} and K. From Figs. 7 and 8, it is found that for Cases IIIa and IVa, which do not build up well-recognized MF, the stratification flow and the layering distribution of T and c_ℓ are broken by the plumes coming from below. The number of plumes of Cases IIIa and IVa is less than that of Case Ia, but the velocity magnitude of the plumes is larger than that of Case Ia. Note that current study cannot suggest a criterion for the formation and stabilization of MF. However, it seems clear that the MF is the outcome of the flow-solidification interaction, more precisely the interaction between the stratification and the plumes.

Interestingly, by influencing the flow, Φ^c_{env} and Φ^c_{circ} influence the solidification in the mush zone. Evolutions of volume-averaged mushy zone quantities for Case I-III are summarized in Figs. 9 and 5(b). The simulation cases with and without the flow were compared. A reduced Φ^c_{env} (Case II) does not influence the total solidification rate significantly. However, a reduced Φ^c_{env} suppresses the columnar envelope growth, i.e., leads to a smaller f_c or larger f_ℓ; and promotes interdendritic solidification, leading to a larger α^c_s (columnar trunks become more massive). An increased Φ^c_{circ} (Case III) is in favour of the columnar envelope growth, i.e., leads to a larger f_c or smaller f_ℓ, and suppresses the interdendritic solidification, i.e., leads to a smaller α^c_s (columnar trunks become more porous). Independent of the above morphological parameters, the flow suppresses the mushy zone, makes the mushy zone denser, and the columnar trunks more massive.

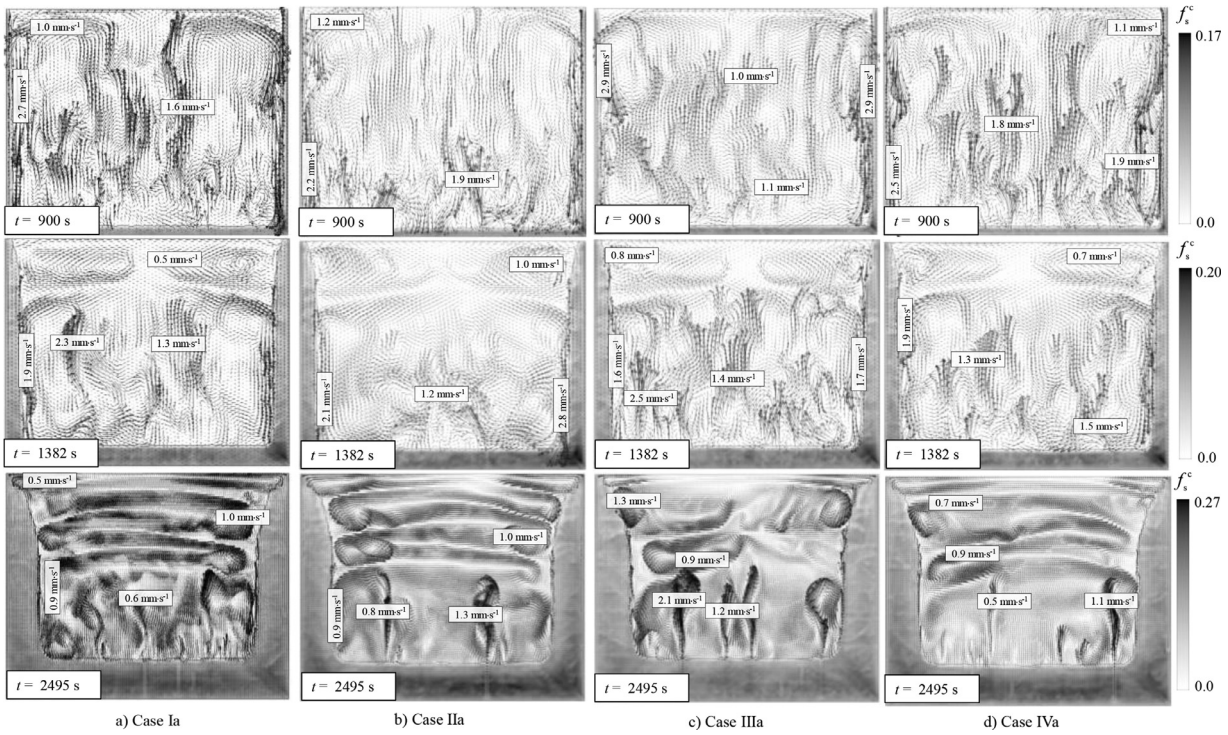

Fig. 7. Effect of morphological parameters of the columnar dendrite envelope on the flow pattern in the bulk. Four simulation cases defined in Table 2 are compared: a) Case Ia; b) Case IIa; c) Case IIIa; and d) Case IVa. The modelling results, f_s^c (grey scale) overlaid with $\vec{u}_\ell$(vectors), are evaluated at three moments corresponding to three typical flow regimes during solidification: 900 s, TU (turbulence); 1382s, TU-ST (turbulence – stratified flow), 2495, MF (meandering flow).

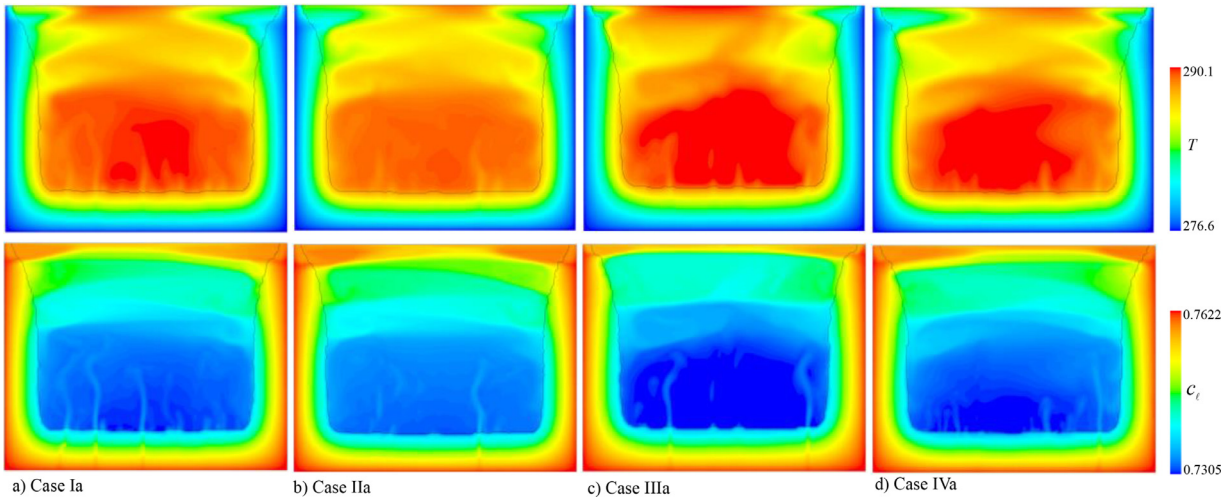

Fig. 8. Effect of morphological parameters of the columnar dendrite envelope on the temperature (upper row) and the liquid concentration (lower row) fields in the bulk at $t = 2495$s. Four simulation cases defined in Table 2 are compared: a) Case Ia; b) Case IIa; c) Case IIIa; and d) Case IVa. (For interpretation of the references to colour in this figure legend, the reader is referred to the web version of this article.)

5.3. Formation of freckle trails

The evolution of freckle trails for Case Ia is shown in Fig. 10. Plumes are formed as a typical double-diffusive convection is induced by the initial solidification from the bottom. Note that the freckle trail does not indicate the presence of an open and stable channel. The difference in f_s^c inside and surrounding the freckle trail is very small. It is difficult to detect the structure of the freckle trail experimentally using a light camera [15]. The plume is measurable using experiments. It is anticipated that one plume roots from one freckle trail. The freckle trails are not stable. Initially, a large number of them are formed from the bottom wall, and they are distributed randomly with a quasi-equal distance. Plumes compete with each other, causing some small freckle trails to die off or merge into a large one. The total number of them decline with time.

In order to understand the formation mechanism of freckle trails, Chen performed an experiment with similar solutions (NH_4Cl – 74 wt.%H_2O and NH_4Cl – 70 wt.%H_2O) [38]. Chen used dye ($KMnO_4$) injection and X-ray tomography methods to observe the flow pattern and fraction solid distribution in the mushy zone during solidification. He reported that 'The upward plume flow in the chimneys (channels) induces a downward flow into the mush, thus reducing the upward flow of the finger convection. As the chimney develops, solid fraction around the rim of the chimney increases. However, *through a mechanism not understood at present*,

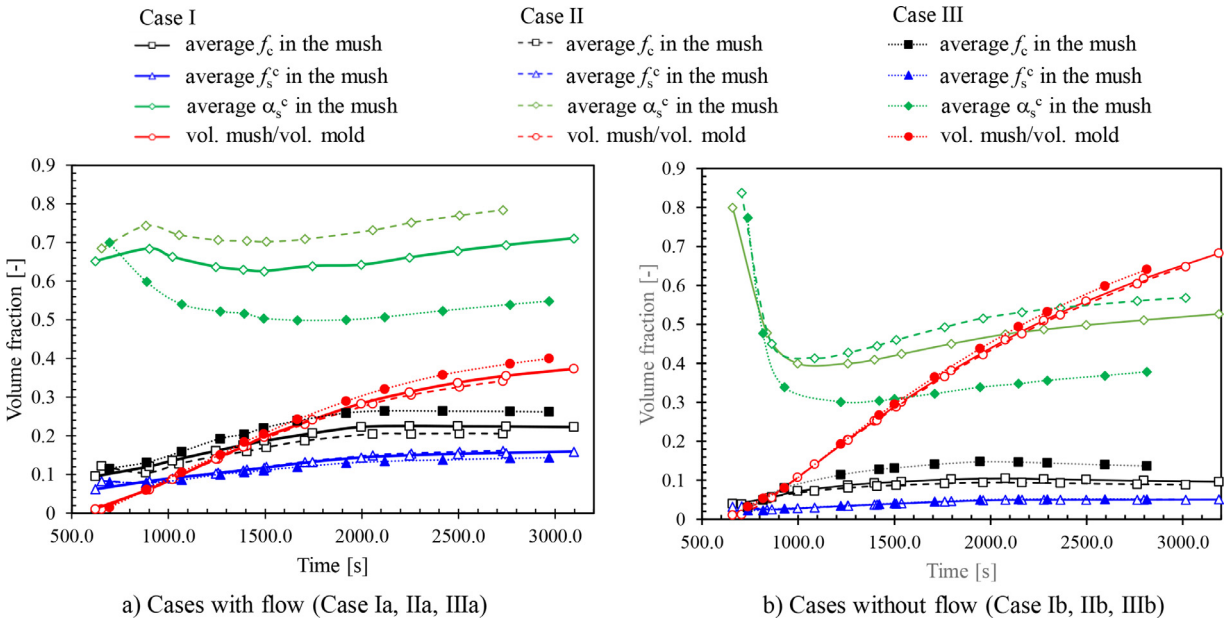

Fig. 9. Effect of morphological parameters of the columnar dendrite envelope on the solidification in the mushy zone. Time evolutions of average f_c, f_s^c, and α_s^c in the mush and the volume ratio of the mush zone region to the entire mould volume are analysed. a) Comparison of simulation cases with flow (Case Ia, IIa, IIIa); b) Comparison of simulation cases without flow (Case Ib, IIb, IIIb).

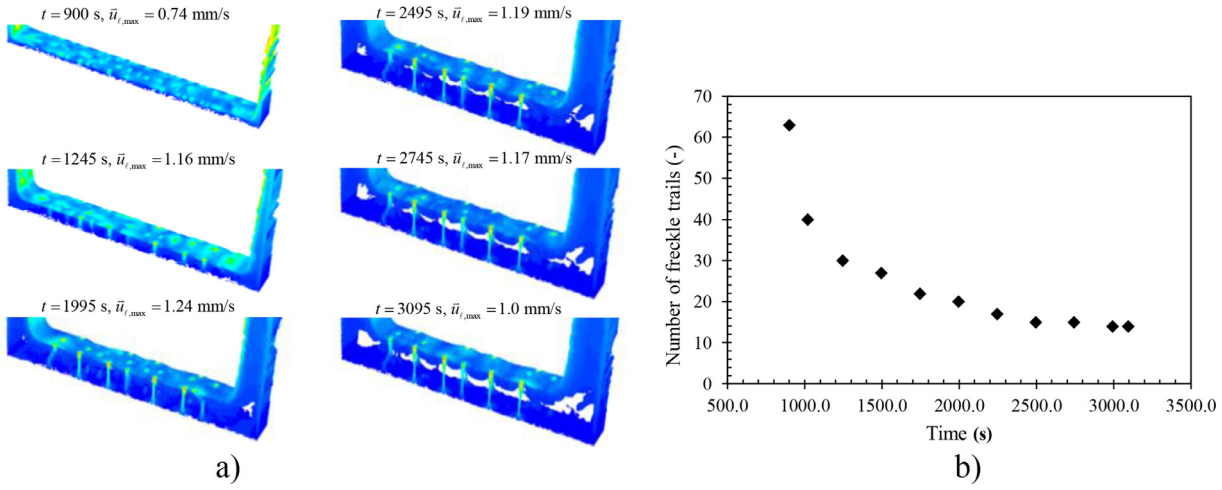

Fig. 10. Evolution of freckle trails (Case Ia). a) Iso-surfaces of $f_s^c = 0.18$, as coloured by $|\vec{u}_\ell|$; b) counts of freckle trails as a function of time. (For interpretation of the references to colour in this figure legend, the reader is referred to the web version of this article.)

the solid fraction at the bottom of the mushy layer remains low. As a consequence, the flow in the chimney is maintained by drawing liquid downward through the mush, then in the horizontal streams along the bottom'. The current modelling results can be used to confirm and explain the above experimental observation. Freckle trails in the current experiment are simulated and shown in Figs. 10 and 11(a). Solidification quantities/parameters along three vertical lines (A, B, and C in Fig. 11(a)) are also shown in Fig. 11(b)-(d). First, the simulation confirms the experimental phenomena that (1) the liquid velocity component in the bottom mushy zone is downward (negative value), except for that which is exactly located in the freckle trails and near the solidification front; (2) the solid fraction increases from the solidification front into the middle of the mush, and it then decreases towards the bottom wall. Secondly, the above *unknown mechanism* for the uneven phase distribution in the mushy zone (lower fraction solid near the casting surface) can be explained. As already described in §5.1, Fig. 6, it is the flow in the mush that modifies the solidification and growth kinetics by adapting the local melt concentration (constitutional undercooling). According to the Flemings' local solute redistribution/conservation theory [39], the flow in the opposite direction to the temperature gradient, i.e. corresponding to the downward flow in the bottom mushy region of the present configuration, should increase the local solidification rate. That is true, if one refers to Fig. 6(f), the solidification rate (M_{ds}^c) in the mushy zone for Case Ia (with flow) is much larger than that of Case Ib (without flow). However, the solidification rate along the solidification direction inside the mushy zone is non-uniform for Case Ia with flow. As shown in Fig. 11(b), exactly at the solidification front the solidification rate (M_{ds}^c) can increase or decrease depending on the flow if it is leaving or entering the mushy zone. In the middle of the mushy, where the flow is mostly downwards, M_{ds}^c reaches its maximum. Then M_{ds}^c decreases towards deep mushy zone until it reaches the wall, where the flow is gradually conducted horizontally, or even reverse its direction. The lowest solidification rate is found near the bottom surface. 'Density reversion' [2], the origin

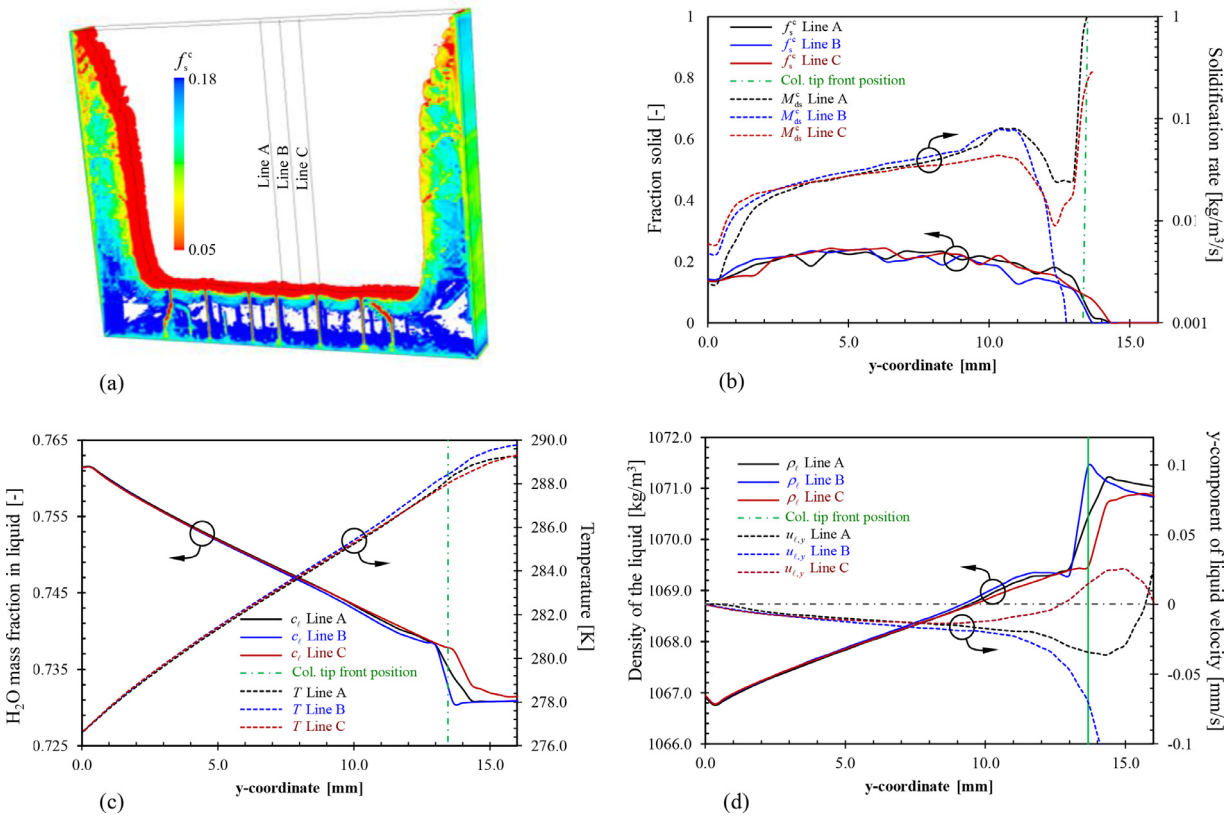

Fig. 11. Freckle trails at 2495s. (a) Iso-surface of f_s^c (= 0.18) indicating the position of the solidification front and freckle trails; (b)-(d) distributions of six different quantities along three vertical lines (Lines A, B, and C, as marked in Fig. (a)) in the y-coordinate direction are shown: fraction solid f_s^c[-], solidification rate M_{ds}^c (kg/m^3/s), H_2O mass fraction in liquid c_ℓ [-], temperature [K], density of the liquid ρ_ℓ [kg/m^3], and velocity component in y-coordinate direction $u_{\ell,y}$ [m/s]. Line C is located in the position of a freckle trail.

and driving force for the plume and freckle trail, can also be verified near the solidification front.

6. Discussions

The reported NH_4Cl – H_2O experiment presents a good example of flow-solidification interaction. Understanding this interaction belongs to a comprehensive research field which includes many subtopics. Few examples of on-going research are mentioned below. Flow can influence the mushy zone thickness [40], lead to macrosegregation of different types [4, 7-8, 30], cause fragmentation [41-42], even modify the microstructure (primary and secondary arm space) [43-44]. The permeability of the mushy zone is a key parameter for the flow calculation. The current paper, through parameter study by comparison of two different permeability formulations [33-34], can only demonstrate its importance. Great research effort has been made on this topic recently [45-50]. As the above phenomena are fully coupled, a comprehensive model is demanded. This paper presents an attempt in this regard.

The NH_4Cl – H_2O experiment was successfully reproduced by a volume-average based model. Despite of some uncertainties regarding to the modelling parameters such as $\Phi^c_{env}$and Φ^c_{circ}, which need further verification, this model provides a new possibility to study the flow-solidification interaction. For example, the experimentally-reported flow regimes in the NH_4Cl – H_2O experiment [15] are well explained; the *unknown mechanism* regarding the formation of freckle trails as reported by Chen [38] is successfully explained. Of course, the model needs further extensions/improvements. The aforementioned $\Phi^c_{env}$and Φ^c_{circ}may be obtained with the assistance of phase field modelling, or determined experimentally with real-time observation (synchrotron X-ray) to track the evolution of the crystal envelope [51]. They may be treated as time-variable quantities. Additionally, the physical properties may be set as temperature even composition dependant. Another point which is not considered in the current simulation cases is the possible formation of equiaxed crystals by fragmentation.

7. Conclusions

A volume-average-based dendritic solidification model is applied to study the flow-solidification interaction during the solidification of an NH_4Cl – 70.43 wt.%H_2O solution in a water-cooled mould with a large sample thickness. Four typical flow regimes, which were experimentally measured using the PIV technique, were quantitatively reproduced by a numerical model. They are (1) pure thermal convection, (2) unstable (turbulent) flow caused by double-diffusive convection, (3) turbulent-stratified flow, and (4) meandering flow. The origin and evolution of the above flow regimes were successfully explained using a numerical model. Some deep insights about the flow-solidification interaction were explored.

- The model has illustrated following flow effect on the developing mushy zone: flow hinders the growth of columnar primary dendrite tips and suppresses the mushy zone, but it speeds up the solidification inside the mushy zone and leads to the formation of a dense mush and massive columnar dendrite trunks. The reason for the above flow effect is (1) the enhanced removal rate of superheat through advection heat transfer, and (2) the transport of solute from the mushy zone into the bulk region by the flow. The latter plays a dominant role.
- Solidification mushy zone of NH_4Cl – H_2O solution is very porous and dendritic. The morphology of the dendrite is de-

scribed by morphological parameters Φ^c_{env} and Φ^c_{circ}. The flow pattern is sensitive to Φ^c_{env} and Φ^c_{circ}. By influencing the flow, Φ^c_{env} and Φ^c_{circ} influence the formation of the mushy zone significantly.

– The proposed model confirmed and explained the results of an experiment that was carried out by Chen to observe the flow in a mushy zone [38]: (1) the flow direction in the bottom mush is in the downward direction, except for that located exactly in the freckle trails; and (2) the solid fraction increases from the solidification front to the middle of the mush, then it decreases towards the bottom wall. The flow in the mush modifies the solidification and growth kinetics by adapting the local melt concentration.

Declaration of Competing Interest

None.

Acknowledgments

This work was financially supported by the Austrian Science Fund (FWF, I 4278-N36), FFG Austrian Space Application Program (ASAP, 859777), FFG Bridge I (868070).

References

[1] R.J. McDonald, J.D. Hunt, Convective fluid motion within the interdendritic liquid of a casting, Metall. Trans. 1 (1970) 1787–1788.
[2] S. Copley, A. Giamei, S. Johnson, M. Hornbecker, The origin of freckles in unidirectionally solidified castings, Metall. Trans. 1 (1970) 2193–2203.
[3] S. Asai, I. Muchi, Theoretical analysis and model experiments on the formation mechanism of channel-type segregation, Trans. ISIJ 18 (1978) 90–98.
[4] M.G. Worster, Convection in mushy layers, Annu. Rev. Fluid Mech. 29 (1997) 91–122.
[5] C.F. Chen, F. Chen, Experimental study of directional solidification of aqueous ammonium chloride solution, J. Fluid Mech. 227 (1991) 567–586.
[6] A. Hellawell, J.R. Sarazin, R.S. Steube, Channel convection in partly solidified systems, Phil. Trans. R. Soc. Lond. A 345 (1993) 507–544.
[7] N. Shevchenko, S. Boden, G. Gerbeth, S. Eckert, Chimney formation in solidifying Ga-25wt pct In alloys under the influence of thermosolutal melt convection, Metall. Mater. Trans. A 44 (2013) 3797–3808.
[8] N. Shevchenko, O. Roshchupkina, O. Sokolova, S. Eckert, The effect of natural and forced melt convection on dendritic solidification in Ga–In alloys, J. Cryst. Growth 417 (2015) 1–8.
[9] F. Cao, F. Yang, H. Kang, C. Zou, T. Xiao, W. Huang, T. Wang, Effect of traveling magnetic field on solute distribution and dendritic growth in unidirectionally solidifying Sn–50 wt%Pb alloy: an in situ observation, J. Cryst. Growth 450 (2016) 91–95.
[10] Y.C. Shih, S.M. Tu, C.C. Chiu, Suppressing freckles during solidification due to periodic motion of top liquid layer, Appl. Therm. Eng. 50 (2013) 1055–1069.
[11] B. Ding, T. Zhou, W. Ren, Y. Zhong, J. Yu, Z. Ren, F. Li, The effect of static magnetic field on the channel formation during directional solidification of aqueous ammonium chloride solution, Cryst. Res. Technol. (2018) 1800113.
[12] C. Beckermann, C.Y. Wang, Equiaxed dendritic solidification with convection: part 3. comparisons with NH_4Cl-H_2O experiments, Metall. Mater. Trans. A 27A (1996) 2784–2795.
[13] A. Kharicha, M. Stefan-Kharicha, A. Ludwig, M. Wu, Simultaneous observation of melt flow and motion of equiaxed crystals during solidification using a dual phase Particle Image Velocimetry technique. Part I: stages characterization of melt flow and equiaxed crystals motion, Metall. Mater. Trans. A 44 (2013) 650–660.
[14] M.G.M. Saffie, F.L. Tan, C.P. Tso, A study on the snowing phenomenon in binary alloy solidification, Appl. Therm. Eng. 50 (2013) 562–571.
[15] M. Stefan-Kharicha, A. Kharicha, M. Wu, A. Ludwig, Observation of the flow regimes and transitions during a columnar solidification experiment, Fluid Dyn. Res. 46 (2014) 041424.
[16] C. Beckermann, R. Viscanta, Mathematical modeling of transport phenomena during alloy solidification, Appl. Mech. Rev. 46 (1993) 1–27.
[17] C. Beckermann, C. Wang, Multiphase/-scale modeling of alloy solidification, Annu. Rev. Heat Trans. 6 (1995) 115–198.
[18] M. Rappaz, P. Thévoz, Solute diffusion model for equiaxed dendritic growth, Acta Metall. 35 (1987) 1478–1497.
[19] M. Rappaz, P. Thévoz, Solute diffusion model for equiaxed dendritic growth: analytical solution, Acta Metall. 35 (1987) 2929–2933.
[20] C. Wang, C. Beckermann, Equiaxed dendritic solidification with convection: part 1. Multi-scale /-phase modeling, Metall. Trans. A 27 (1996) 2754–2764.
[21] M. Wu, A. Fjeld, A. Ludwig, Modeling mixed columnar-equiaxed solidification with melt convection and grain sedimentation-Part I: model description, Comp. Mater. Sci. 50 (2010) 32–42.
[22] M. Wu, A. Ludwig, A. Fjeld, Modeling mixed columnar-equiaxed solidification with melt convection and grain sedimentation-Part II: illustrative modeling results and parameter studies, Comp. Mater. Sci. 50 (2010) 43–58.
[23] L. Sturz, M. Wu, G. Zimmermann, A. Ludwig, M. Ahmadein, Benchmark experiments and numerical modelling of the columnar-equiaxed dendritic growth in the transparent alloy Neopentylglycol-(d)Camphor, IOP Conf. Series: Mater. Sci. Eng. 84 (2015) 012086.
[24] M. Ahmadein, M. Wu, J. Li, P. Schumacher, A. Ludwig, Prediction of the as–cast structure of Al-4.0 wt.% Cu ingots, Metall. Mater. Trans. A 44 (2013) 2895–2903.
[25] M. Ahmadein, M. Wu, A. Ludwig, Analysis of macrosegregation formation and columnar-to-equiaxed transition during solidification of Al-4 wt.%Cu ingot using a 5-phase model, J. Cryst. Growth 417 (2015) 65–74.
[26] S. Felicelli, D. Poirier, J. Heinrich, Modeling freckle formation in three dimention during solidification of multicomponent alloys, Metall. Mater. Trans. B 29 (1998) 847–855.
[27] S. Felicelli, J. Heinrich, D. Poirier, Three-dimentional simulations of freckles in binary alloys, J. Cryst. Growth 191 (1998) 879–888.
[28] J. Guo, C. Beckermann, Three-dimentional simulation of freckle formation during binary solidification: effect of mesh spacing, Num. Heat Transf. Part A 44 (2003) 559–576.
[29] R. Katz, M. Worster, Simulation of directional solidification, thermochemical convection, and chimeney formation in Hele-Shaw cell, J. Comput. Phys. 227 (2008) 9823–9840.
[30] M. Wu, A. Ludwig, A. Kharicha, Volume-averaged modeling of multiphase flow phenomena during alloy solidification, Metals 9 (2019) 229 doi:10.3390.
[31] M. Wu, M. Stefan-Kharicha, A. Kharicha, A. Ludwig, Numerical investigation of an in-situ observed flow regimes during solidification of an NH_4Cl–70 wt.%H_2O solution, IOP Conf. Series: Mater. Sci. Eng. 861 (2020) 012041.
[32] J. Lipton, M. Glicksman, W. Kurz, Dendritic growth into undercooled alloy metals, Mater. Sci. Eng. 65 (1984) 57–63.
[33] J. Ramirez, C. Beckermann, Evaluation of a Rayleigh Number Based Freckle Criterion for Pb-Sn and Ni-base Superalloys, Metall. Mater. Trans. A 34 (2003) 1525–1536.
[34] A. Noeppel, A. Ciobanas, X.D. Wang, K. Zaidat, N. Mangelinck, O. Budenkova, A. Weiss, G. Zimmermann, Y. Fautrelle, Influence of forced/natural convection on segregation during the directional solidification of Al-based binary alloys, Metall. Mater. Trans. 41 (2010) 193–208.
[35] M. Stefan-Kharicha, A. Kharicha, Wu M. Mogeritsch, A. Ludwig, Review of Ammonium Chloride–Water Solution Properties, J. Chem. Eng. Data 63 (2018) 3170–3183.
[36] A. Ramani, C. Beckermann, Dendrite tip growth velocities of settling NH_4Cl equiaxed crystals, Scr. Mater. 36 (1997) 633–638.
[37] R. Perry, D. Green, J. Maloney, Perry's Chem. Engineers' Handbook, 7th ed., The McGraw-Hill Companies, New York, 1999.
[38] C.F. Chen, Experimental study of convection in a mushy layer during directional solidification, J. Fluid Mech. 293 (1995) 81–98.
[39] M.C. Flemings, Our understanding of macrosegregation: past and present, ISIJ Int. 40 (2000) 833–841.
[40] H. Zhang, M. Wu, Y. Zheng, A. Ludwig, A. Kharicha, Numerical study of the role of mush permeability in the solidifying mushy zone under forced convection, Mater. Today Comm. 22 (2020) 100842.
[41] R. Mathiesen, L. Arnberg, P. Bleuet, A. Somogyi, Crystal fragmentation and columnar-to-equiaxed transitions in Al-Cu studied by synchrotron X-ray video microscopy, Metall. Mater. Trans. A 37 (2006) 2515–2524.
[42] E. Liotti, A. Lui, S. Kumar, Z. Guo, C. Bi, T. Connolley, P. Grant, The spatial and temporal distribution of dendrite fragmentation in solidifying Al-Cu alloys under different conditions, Acta Mater. 121 (2016) 384–395.
[43] S. Steinbach, L. Ratke, The effect of rotating magnetic fields on the microstructure of directionally solidified Al–Si–Mg alloys, Mater. Sci. Eng. A 413-414 (2015) 200–204.
[44] T. Takaki, S. Sakane, M. Ohno, Y. Shibuta, T. Aoki, Large-scale phase-field lattice Boltzmann study on the effects of natural convection on dendrite morphology formed during directional solidification of a binary alloy, Comp. Mater. Sci. 177 (2020) 109581.
[45] D. Bernard, Ø. Nielsen, L. Salvo, P. Cloetens, Permeability assessment by 3D interdendritic flow simulations on microtomography mappings of Al–Cu alloys, Mater. Sci. Eng. A 392 (2005) 112–120.
[46] A. Ludwig, A. Kharicha, C. Hölzl, J. Domitner, M. Wu, T. Pusztai, 3D Lattice Boltzmann flow simulations through dendritic mushy zones, Eng. Analy. Bound. Elem. 45 (2014) 29–35.
[47] E. Khajeh, D.M. Maijer, Physical and numerical characterization of the near-eutectic permeability of aluminum–copper alloys, Acta Mater. 58 (2010) 6334–6344.
[48] T. Takaki, S. Sakane, M. Ohno, Y. Shibuta, T. Aoki, Permeability prediction for flow normal to columnar solidification structures by large-scale simulations of phase-field and lattice Boltzmann methods, Acta Mater. 164 (2019) 237–249.
[49] C. Puncreobutr, A.B. Phillion, J.L. Fife, P.D. Lee, Coupling in situ synchrotron X-ray tomographic microscopy and numerical simulation to quantify the influence of intermetallic formation on permeability in aluminium–silicon–copper alloys, Acta Mater. 64 (2014) 316–325.
[50] Y. Feng, M. Zaloznik, B.G. Thomas, A.B. Phillion, Meso-scale simulation of liquid feeding in an equiaxed dendritic mushy zone, Materialia 9 (2020) 100612.
[51] M. Ahmadein, M. Wu, G. Reinhart, H. Nguyen-Thi, A. Ludwig, Modelling Al-4 wt.%Cu as-cast structure using equiaxed morphological parameters deduced from in-situ synchrotron X-ray radiography, IOP Cof. Series: Mater. Sci. Eng. 117 (2016) 012010.